2019-03-26

Ka-band Planar Vivaldi Antenna with a Core for High-Gain

Manh ha Hoang
Technological University Dublin, manhha.hoang@mydit.ie

Kansheng Yang
Technological University Dublin

Matthias John
Technological University Dublin, matthias.john@tudublin.ie

See next page for additional authors

Recommended Citation

Hoang, M. Ha, et al. "Ka-band Planar Vivaldi Antenna with a Core for High-Gain", IET Microwaves, Antennas & Propagation, vol. 13, no. 6, pp. 732-735, 2019. DOI: 10.1049/iet-map.2018.5834

Funder: SFI

Ka-band Planar Vivaldi Antenna with a Core for High-Gain

Ha Hoang*, Kansheng Yang, Matthias John, Patrick McEvoy, Max J. Ammann

Antenna and High-Frequency Research Centre – Dublin Institute of Technology, Dublin, Ireland
*manhha.hoang@mydit.ie

Abstract: A planar Vivaldi antenna structure with a core element is proposed for high gain. Techniques to achieve a significant gain improvement over the full Ka (24-40 GHz) band are implemented; including a frequency-independent excitation method, the introduction of logarithmic ripple on the lateral edges and enclosing the antenna in a dielectric material.

1. Introduction

Most of radiating electromagnetic (EM) energy from Vivaldi antennas is from their tapered slot structure in travelling wave modes which provides moderately high gain in the end-fire direction with wide bandwidth characteristics. Availability of low-cost planar fabricating technology is also an advantage of these simple antenna structures. Hence, there is a wide range of applications for these antennas, which include the emerging 5G systems and UWB radar/ sensing/ imaging systems.

However, the gain of conventional planar Vivaldi antennas is limited, even when the length of the antenna is increased. There have been some works reported tackling the problem of limited Vivaldi antenna gain. In [1], a dielectric-load structure was used for a Ka-band Vivaldi antenna, while [2] reported that anisotropic zero-index metamaterials (ZIM) were added in the aperture of a UWB Vivaldi antenna to improve gain. In [3] and [4], double-slot and double-antipodal structures were employed for this purpose. In [5] and [6], a parasitic elliptical element was added to improve gain as well as expand beamwidth for the antennas. The antenna gain was increased by using a half-elliptical shape for the substrate at the radiating aperture which plays the role of a lens [7]. And in [8] with a 3D structure extended from [7], the antenna was surrounded by a dielectric structure for significant enhancement of gain.

In this work, a hybrid Vivaldi structure with a core element for high gain is proposed [9]. A study of excitation methods for this structure to provide a wideband balanced field distribution is presented. The effectiveness of using the core element for gain improvement is examined. Previously reported techniques for improvement of Vivaldi antennas are integrated on this structure such as the addition of lateral edge ripples, the addition of lens to the radiating aperture and surrounding the antenna by a dielectric structure.

2. Antenna Structure and Excitation Methods

2.1. Vivaldi structure with a core element

The proposed antenna structure is shown in Fig. 1. With the core element, this coplanar structure possesses a combination of structural features of a double-slot Vivaldi antenna and a Vivaldi antenna with a parasitic element.

The initial structure has two main parts including a ground zone with two symmetrical exponential curves and a core element arranged to have a parasitic coupling to ground.

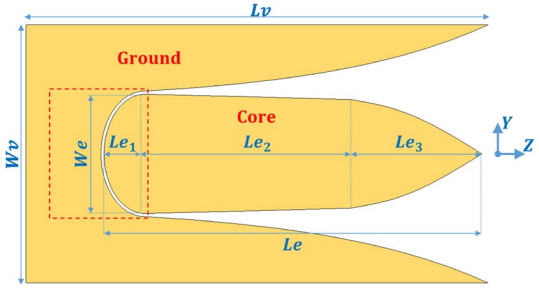

Fig. 1. *Initial Vivaldi antenna structure with a core element. The area marked in red is the feed region shown in Fig. 2*

The core is divided into three sub-parts. The first one is a half ellipse with a minor-axis length $2\times Le_1$ and a major-axis length We which is close to the ground to create a slot line with a slot gap s_g. The second sub-part with the length Le_2 has two exponential curves opposite to the ground. These two pairs of exponential curves create a double Vivaldi slot structure.

The equation describing the curve on the ground is:

$$y = e^{p_v z} - 1 + \frac{W_e}{2} + s_g\,, \qquad 0 \le z \le Lv_{curve}$$

with the core element described by:

$$y = -e^{p_e z} + 1 + \frac{W_e}{2}\,, \qquad 0 \le z \le Le_2$$

where p_v =0.075, p_e=0.023 and Lv =27.5mm.

The p_v-factor of the ground exponential curves is chosen based on the Lv, Wv, We and s_g parameters and the core exponential factor p_e is chosen depending on the Le_2, We and s_g parameters. The last subpart of the core is an extension from the second one with the length Le_3 created from two spline curves which meet at the centre. The parameters of the structure are shown in Table 1.

Table 1 Parameters of the initial structure

Parameters	Value
Wv	*20.56 mm*
Lv	*37.00 mm*
Le	*30.25 mm*
Le_1	*3.34 mm*
Le_2	*16.41 mm*
Le_3	*10.50 mm*
We	*9.50 mm*
s_g	*0.25 mm*

This antenna is designed on RT5880 (ε_r=2.2 and tanδ=0.0009 @10GHz) material with 0.25 mm thickness-*h* and two copper layers with 0.0017 mm thickness-*t*.

2.2. Study of excitation methods

With planar fabricating technology, excitation for the slot based on open-end stub structure is an appropriate solution. Excitation method-I for the slot is described in Fig. 2(a). The slot is excited by a microstrip line network (50Ω dividing into two 100Ω lines, of 0.78 and 0.19 mm width respectively) built on the top copper layer (darker colour, compared to the bottom layer of the ground and core)

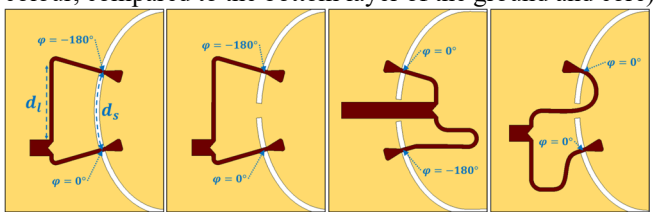

(a) (b) (c) (d)

Fig. 2. *Excitation method-I (a), II (b), III (c) and IV (d)*

with two open-end stubs crossing over the slot from the ground zone. These stubs are placed symmetrically from the centre, and the microstrip lines are fed from a T-divider. To ensure the field vectors distribution at the two radiating apertures corresponding to the two Vivaldi slots is balanced and the field vectors are in the same direction, not eliminating each other, the requirement of the signal phase at the crossing points of the two stubs are 180° out of phase. In this work, to tackle this requirement, the electrical length difference of the two microstrip lines feeding the stubs d_l is chosen an electrical half wavelength at the operating frequency. Furthermore, to prevent cancellation of fields on the slot, the electrical length of the slot line segment between the stubs d_s is also chosen to be a half wavelength.

With this excitation method, the distribution of E-field magnitudes on the metal plane of the ground and core at the operating frequency is examined and shown in Fig. 3(a). This shows that besides demonstrating that the field distribution is balanced, the potential difference between the core and the ground zone is eliminated at the slot centre position (symmetrical axis) because of the structural symmetry and the opposite excitation condition. This feature is taken advantage of in the next step of excitation-structure design.

Fig. 2(b) shows the excitation method-II with a small modification in the structure from excitation method-I. There is a small conducting strip of 0.67 mm width placed between the ground zone and the core at the slot centre, d_s remains the same. Fig. 3(b) shows the E-field on the metal plane of the antenna. This result demonstrates that the fields are the same as excitation method-I. Thus, the connecting strip between the ground and the core does not affect the mode on the slot. This connection is a vital condition for energy transfer from

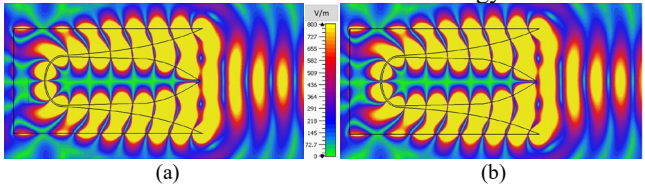

(a) (b)

Fig. 3. *E-field distribution on the antenna with excitation method-I (a) and excitation method-II (b) at 33GHz*

outside of the core zone across the slot into the inside without affecting the mode, and it is pivotal to develop further excitation methods.

Fig. 2(c) shows another excitation structure. Method-III is like an inverse of the method-II in which the main microstrip line transfers EM energy from the ground zone into the core zone based on the connecting strip. Then, it is divided to feed the slot using two stubs. These stubs cross the slot from the core zone, and their signals at the crossing positions also need a 180° difference in phase (at the centre frequency), so a half wavelength difference in electrical length of the two feed lines is also maintained for this method.

Because of existence of a half wavelength difference in electrical length of the two feed lines at the operating frequency in excitation methods -I, -II and -III, a change in the operating frequency leads to a degradation of the 180^0-phase shift at the two stubs and this leads to an unbalance in

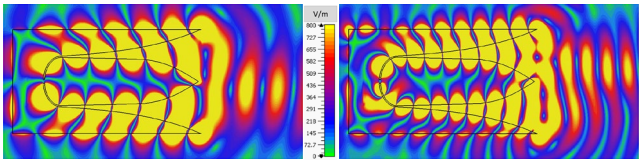

(a) (b)

Fig. 4. *Unbalance of E-field distribution on the antenna with excitation method-II at 26GHz (a) and 39GHz (b)*

field distribution on the two Vivaldi slots. Fig. 4 shows two examined results proving this with the method-II at a lower frequency and an upper frequency compared to the designed operating frequency.

Excitation method-IV shown in Fig. 2(d) employs two stubs crossing the slot from opposite directions. One is from the ground zone, and another one is from the core zone. The conducting strip supports EM energy transfer to the second one.

With this opposing stub arrangement, there is no need for a 180° phase shift at the crossing positions of the two stubs, so the electrical lengths of the two feed lines are equal. This presents a major benefit for excitation method-IV; that is a

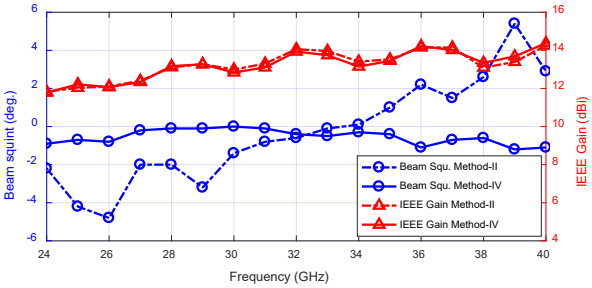

Fig. 5. *Beam-squint in the E-plane (YZ) and maximum IEEE-gain vs. frequency for excitation method-II and IV.*

balanced field distribution on the two Vivaldi slots which is maintained across a wide frequency range.

An examination verifying this is implemented. Because the z-axis is an axis of symmetry of the main-radiating structure in the YZ plane (see Fig. 1) and $+z$ is the expected radiating direction, any imbalance of near-field distribution on the structure will impact the far-field. This will generate YZ plane beam squint off the $+z$ direction. So, instead of assessing the field distribution balance based on observing complex near-field distribution at each frequency, the far-field beam-squint characteristic in the YZ plane is used for this purpose. The maximum IEEE-gain characteristic

is also used to assess the excitation method-II and IV over the whole Ka-band. This is because it includes both directivity and efficiency.

The results in Fig. 5 show that there is a significant imbalance at the lower and upper frequencies for excitation method-II. The beam-squint range is greater than 10^0, while the excitation method-IV presents a good field balance across the full Ka-band with a superior beam-squint performance and only a 1^0-beam-squint range. Additionally, the maximum IEEE-gain result also presents equivalence in maximum directivity and no significant difference in efficiency over the full frequency band of the antenna when using the two excitation methods.

With its better performance, the excitation method-IV is used in the next steps of the design process.

3. Gain Improvement

In the first stage of the gain improvement process, the antenna size is increased in length *Lv* and width *Wv*. Specifically, *Lv* is increased to 71 mm, and *Wv* is increased to 31 mm. The new size structure is shown in Fig. 6.

3.1. Role of the core in improving gain

The core element is an important part of the antenna structure. It disperses EM energy into two parts on the two Vivaldi slots, and this leads to wavefronts through the radiating aperture which is formed closer to a plane wave compared to a semi-spherical wave of a single-Vivaldi-slot antenna with the same radiating aperture width. This is an important factor contributing to the high gain of the antenna. An investigation to examine how the core element impacts the antenna performance is made by characterising the gain versus the core length. Fig. 6 illustrates changes in the core in length *Le* from 30.25 mm to 80.25 mm with six steps. The result in Fig. 7 demonstrates a trend in increased gain with increased core length.

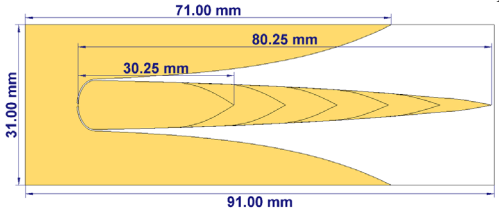

Fig. 6. *Expansion in size and change in core length.*

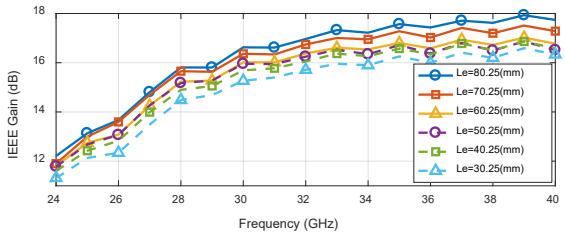

Fig. 7. *Dependence of gain on core length.*

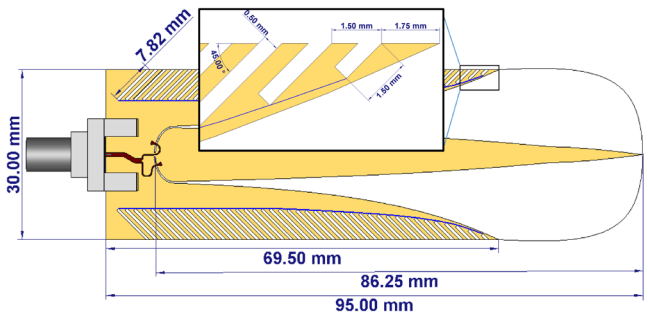

Fig. 8. *Structure with ripples at the lateral edges.*

3.2. Integrating other techniques

In this section, some other techniques are employed to enhance gain.

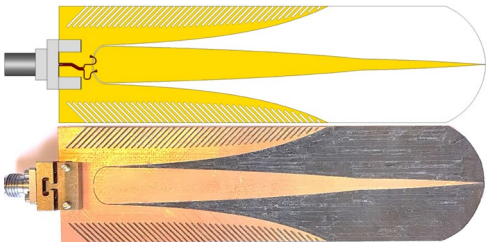

Fig. 9. *Prototype structure in top and bottom view.*

- *Ripple on the lateral edges*

A ripple arrangement on each lateral edge was introduced using 41 slots with slot depths obeying a logarithmic curve defined by:

$$depth(i) = \begin{cases} depth_0 + ln[A(i-1)^p + 1], & i = 1, \dots, N_1 \\ depth(N_1), & i = N_1 + 1, N_1 + 2, \dots, N_2 \end{cases}$$

with $depth_0$=1.5mm, A=2.12, p=1.8, N_1=23, N_2=41.

Depth, position, distance and rotating angle parameters of the slots are optimised for best gain. As well as this, the antenna size is also increased, and the substrate edges at the radiating aperture are reshaped by a spline curve to play the role of a lens at the aperture as illustrated in Fig. 8.

The simulation results show that the maximum gain of this planar structure (95×30 mm^2) reached 19.3 dBi and increasing the length to 110 mm provided 19.9 dBi gain.

An antenna prototype with the size of 110×30 mm^2 was fabricated as shown in Fig. 9. Simulation and measurement results for this prototype are shown in Fig. 10.

Table 2 Comparison of planar structures

Antennas	Frequency (GHz)	Max. Gain (dBi)	Sizes (mm^3)
[3]	2.5-15	*14.5*	*150×80×1*
[4]	4.7-20	*14.8*	*166×70×0.76*
[1]	Ka band	*13.2*	*59×8×0.5*
[7],[8]	5-50	*16.5*	*95×30×0.5*
Proposed	Ka band	*19.5*	*110×30×0.25*

The measurement results illustrate that the matching characteristic of the antennas is good over the full Ka-band 24-40 GHz and maximum gain reaches 19.5 dBi and is better than 17 dBi over the full Ka-band. Radiation patterns of the antenna present good agreement between simulation and measurement.

A comparison of maximum gain of the proposed antenna with previously reported works are shown in Table 2 and shows that maximum gain of this antenna is greater than other reported planar structures.

- *Surrounding the antenna by a dielectric*

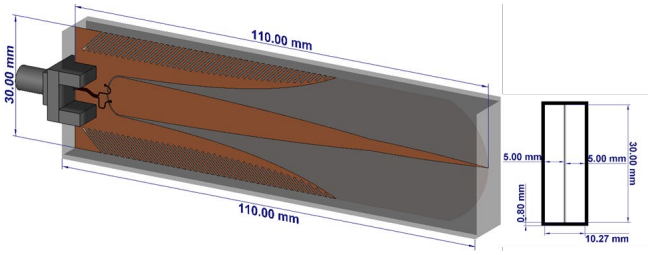

Fig. 11. *Structure surrounded by dielectric.*

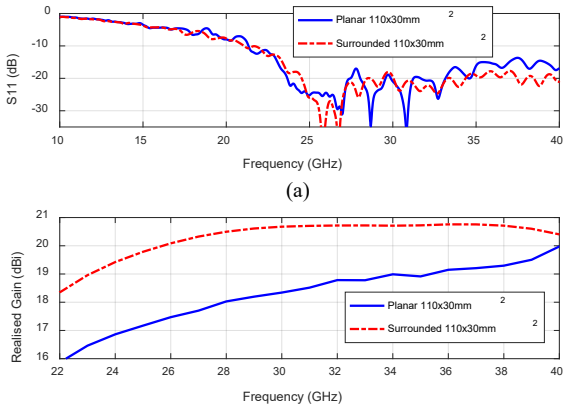

Fig. 12. Effect of dielectric enclosure on *S11 (a), realised gain (b).*

An extension of this planar structure into a 3D structure is also implemented by surrounding the structure by Teflon-dielectric flat sheets with 0.8 mm thickness as introduced in [8]. This is structured like a rectangular waveguide, and the enclosed antenna structure is shown in Fig. 11.

Simulation results in Fig. 12 show a significant gain improvement for the enclosed structure with a maximum gain of 20.8 dBi. They also reveal the S11 to be stable with the dielectric enclosure.

4. Conclusion

The proposed planar Vivaldi antenna structure with the core element combines advantages of the double-slot Vivaldi structure and advantages of the parasitic element to increase the maximum gain range for the planar Vivaldi antenna type. The excitation for the structure was studied, and a wideband-balanced excitation method was selected to contribute significantly to the performance in gain, bandwidth and pattern. Integrating the new ripple structure on the lateral edges and the lens at the radiating aperture of the planar structure improve further the gain performance. The extension into a 3D structure by dielectric enclosure also adds a significant gain improvement.

5. Acknowledgements

This publication has emanated from research conducted with the financial support of Science Foundation Ireland (SFI) and is co-funded under the European Regional Development Fund under Grant Number 13/RC/2077.

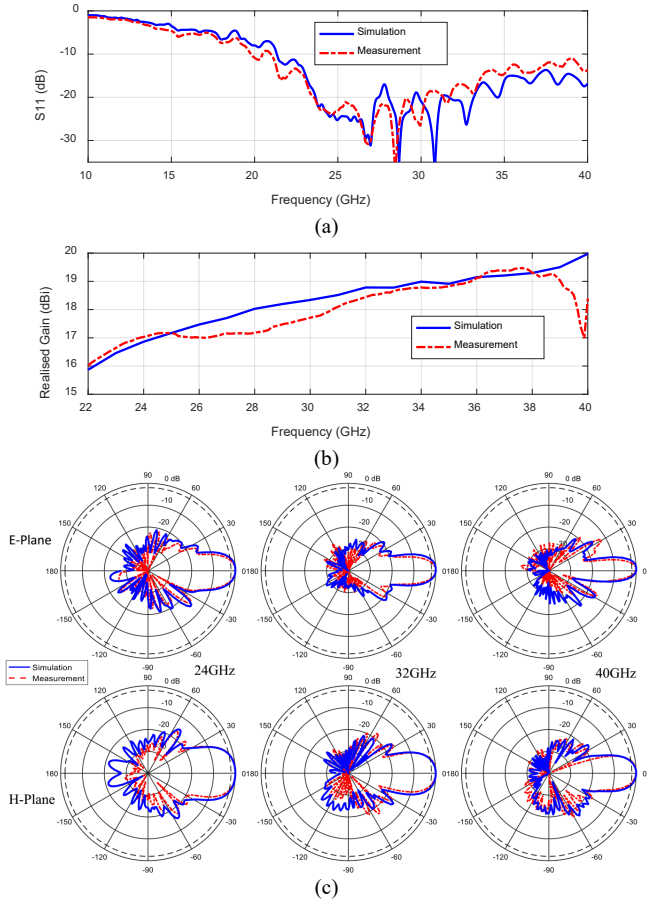

Fig. 10. *Simulation and measurement results of the prototype, S11 (a), realised gain (b) and pattern (c).*

6. References

[1] J. Puskely, J. Lacik, Z. Raida, and H. Arthaber, 'High Gain Dielectric-Loaded Vivaldi Antenna for Ka-Band Applications', *IEEE Antennas Wireless* Propag. Lett., vol. 15, pp. 20042007, 2016.

[2] B. Zhou and T. J. Cui, Directivity Enhancement to Vivaldi Antennas Using Compactly Anisotropic

ZeroIndex Metamaterials', *IEEE Antennas Wireless* Propag. Lett., vol. 10, pp. 326-329, 2011.
[3] Y.-W. Wang, G.-M. Wang, and B.-F. Zong, 'Directivity Improvement of Vivaldi Antenna using Double-Slot Structure', *IEEE Antennas Wireless* Propag. Lett., vol. 12, pp. 1380-1383, 2013.
[4] Y. Zhang, E. Li, C. Wang, and G. Guo, 'Radiation Enhanced Vivaldi Antenna with Double-Antipodal Structure', *IEEE Antennas Wireless* Propag. Lett., vol. 16, pp. 561-564, 2017.
[5] I. T. Nassar and T. M. Weller, 'A Novel Method for Improving Antipodal Vivaldi Antenna Performance', IEEE Trans. on Antennas and Propag., vol. 63, no. 7, pp. 3321-3324, 2015.
[6] K. Yang, A. Loutridis, X. Bao, P. McEvoy, and M. J. Ammann,: 'A coplanar Vivaldi Antenna with Integrated Filter for Ka-band', in *Antennas &* Propag. Conf. (LAPC), 2016 Loughborough, pp. 1-4, 2016.
[7] Mahdi Moosazadeh, Sergey Kharkovsky, Joseph T. Case, Bijan Samali,: 'Improved Radiation Characteristics of Small Antipodal Vivaldi Antenna for Microwave and Millimeter-Wave Imaging Applications', *IEEE Antennas Wireless Propag. Lett*., vol. 16, pp. 1961-1964, 2017.
[8] Mahdi Moosazadeh, 'High-Gain Antipodal Vivaldi Antenna Surrounded by Dielectric for Wideband Applications', *IEEE Trans. on Antennas and Propag*., vol. 66, no. 8, pp. 4349-4352, 2018.
[9] H. Hoang, K. Yang, M. John, P. McEvoy, and M. J. Ammann,: 'Ka-band Vivaldi antenna with novel core element for high-gain', in *Antennas &* Propag. Conf. (LAPC), 2017 Loughborough, pp. 1-4, 2017.